Energetics of a Possible Proton Exit Pathway for Water Oxidation in Photosystem II†

Hiroshi Ishikita,‡ Wolfram Saenger, Bernhard Loll,§ Jacek Biesiadka, and Ernst-Walter Knapp*

Institute of Chemistry and Biochemistry, Department of Biology, Chemistry, and Pharmacy, Free University of Berlin, Takustrasse 6, D-14195 Berlin, Germany

Received August 13, 2005; Revised Manuscript Received December 23, 2005

ABSTRACT: The crystal structure of photosystem II (PSII) at 3.0-Å resolution suggests that titratable residues on the lumenal side of D1/D2 and PsbO form a polar channel, which might serve as a proton exit pathway associated with water oxidation on the Mn-cluster. With full account of protein environment, we calculated the pK_a of these residues by solving the linearized Poisson−Boltzmann equation. Along the prospective proton channel, the calculated pK_a of titratable residues (namely via D1-Asp61, D1-Glu65, D2-Glu312, D2-Lys317 D1-Asp59, D1-Arg64, PsbO-Arg152, and PsbO-Asp224) monotonically increase from the Mn-cluster to the lumenal bulk side. We suggest that these residues form the exit pathway guiding protons, which are released at the Mn-cluster as a product of water oxidation, in an exergonic process out of PSII. Upon the S2 to S3 transition, CP43-Arg357 showed a dramatic deprotonation of ca. one H^+, suggesting that this residue is coupled to the redox states of the Mn-cluster and the tyrosine Y_Z. The calculated pK_a values of 4.2−4.4 for D2-Glu312 and those of ∼8−10.9 for D1-Asp59 and D1-Arg64 are indicative of the experimentally determined pK_a values for inhibition of S-state transitions. Upon removal of the atomic coordinates of PsbO, the pK_a of these residues are dramatically affected, indicating a significant role of PsbO in tuning the pK_a of those residues in the proton exit pathway.

Atmospheric oxygen is generated by water oxidation at the Mn-cluster of the photosynthetic protein−pigment complex, photosystem II (PSII) located in the thylakoid membrane of cyanobacteria, green algae, and plants. The photosynthetic reaction in PSII is initialized by light absorption, resulting in electronic excitation that is ultimately converted to chemical potential by a charge separation process at the P680 chlorophyll *a* (Chl*a*)[1] of the PSII reaction center. Charge separation leads to formation of an oxidized positively charged radical, $P680^+$. In intact PSII, $P680^+$ is rereduced by the redox-active tyrosine D1-Tyr161 (Y_Z), which is subsequently reduced by an electron from the Mn-cluster close to the lumenal (pepriplasmic) side of the membrane. Sequential excitations of P680 drive the redox state of the Mn-cluster from the lowest S0 to the highest oxidized state S4. The resulting accumulation of positive charge is expected to have a dramatic impact on the protonation pattern close to the Mn-cluster. As a product of water oxidation, molecular oxygen (O_2) evolves during the S3 to S0 transition i.e., in the transient S4 state, which has not been resolved in spectroscopic studies (reviewed in ref *1*). As a hydrogen bond (H-bond) partner, Y_Z has D1-His190, while the symmetrical counterpart D2-Tyr160 (Y_D) has D2-His189. The apparent proximity of Y_Z to the Mn-cluster (edge-to-edge distance between Mn-cluster and Y_Z is 5 Å (*2*)) and its redox activity indicates its significant role in water oxidation at the Mn-cluster.

A number of mechanisms have been proposed for the redox reaction between P680 and the Mn-cluster. It is a matter of debate whether the role of Y_Z in water oxidation is to function as a hydrogen abstractor (*3*, *4*) or electrostatic promoter (*5*). The existence of an exit pathway of protons released upon water oxidation without involving Y_Z and D1-His190 (proton exit pathway) was first suggested by Haumann and Junge (*6*). Connected to the Mn-cluster, a channel of polar residues starts at D1-Asp61 and precedes about 15 Å toward the docking site of PsbO on the lumenal surface, as suggested by Barber, Iwata, and co-workers (*7*−*10*) (Figure 1). PsbO has a cylindrical β-barrel shape, but its interior is filled by hydrophobic residues, including seven bulky phenylalanines. Therefore, this protein is unlikely to function as a tube that channels water or protons (*9*, *10*). Instead, a cluster of hydrophilic residues from the D1/D2 proteins located at the entrance of the PsbO tube seems to function as a proton exit pathway with an overall length of about 35 Å consisting of D1-Asp61, D1-Glu65, D2-Glu312, D2-Lys317 (*7*, *8*), PsbO-Asp158, PsbO-Asp222, PsbO-Asp223, PsbO-Asp224, PsbO-His228, and PsbO-Glu229 (*9*,

† This work was supported by the Deutsche Forschungsgemeinschaft SFB 498, Projects A4 and A5, Forschergruppe Project KN 329/5−1/5−2, GRK 80/2, GRK 268, GRK 788/1. H.I. was supported by the DAAD.

* Corresponding author. Tel: (+ 49)30-83854387. Fax: (+ 49)30-83856921. E-mail: knapp@chemie.fu-berlin.de.

‡ Current address: Department of Chemistry, The Pennsylvania State University, 104 Chemistry Building, University Park, PA 16802 (e-mail: hiro@chemie.fu-berlin.de).

§ Current address: Max-Planck-Institut für Medizinische Forschung, Abteilung für Biomolekulare Mechanismen, 69200 Heidelberg, Germany.

[1] Abbreviations: bRC, bacterial photosynthetic reaction center; Chl*a*, chlorophyll *a*; LPB equation, linearized Poisson−Boltzmann equation; Mn-cluster, oxygen-evolving complex with Mn ions; Pheo*a*, pheophytin *a*; PSII, photosystem II; Q, plastoquinone; $Y_{Z/D}$, redox active tyrosine D1-Tyr161/D2-Tyr160.

10.1021/bi051615h CCC: $33.50
Published on Web 01/27/2006

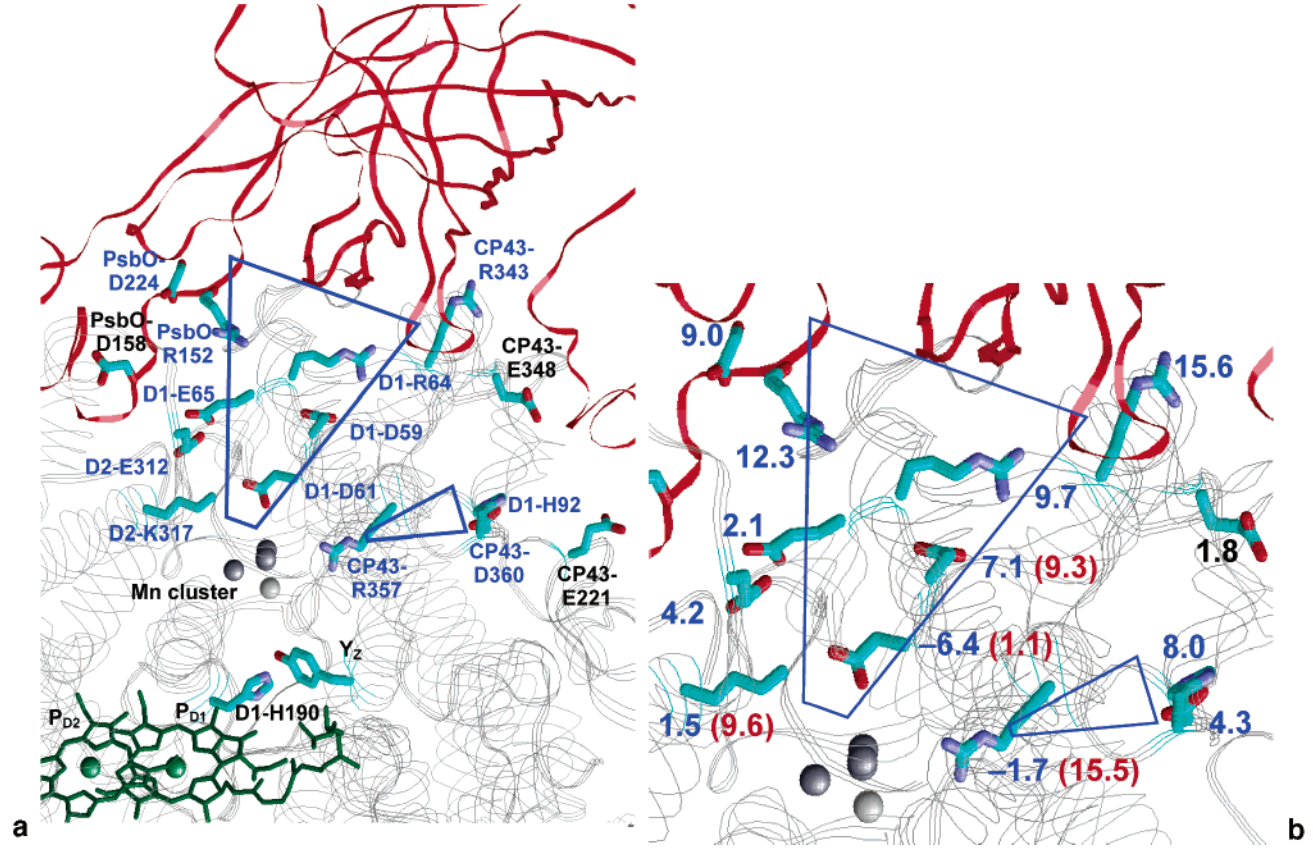

FIGURE 1: (a) Hydrophilic channels at the lumenal side of PSII based on the 3.0-Å structure (*2*), with the lumenal side of the membrane on top. Proton exit channel indicated schematically as a large wedge and the water entry channel as a small wedge, respectively. Residues whose involvements in the proton exit pathway are highly probable based on the calculated pK_a in the present study are labeled blue. PsbO is depicted as a red ribbon. The blue lines mark the regimes of the proton exit pathway. For the sake of clarity, the other extrinsic proteins PsbU and PsbV are not shown. (b) Calculated pK_a values in the S4 state (colored in either blue or black) and in the S0 state (colored in red). The latter pK_a values are shown only for those residues that show significant differences (by more than 2) between the S0 and the S4 state.

10), without involving Y_Z and D1-His190. This channel may not only provide the proton exit pathway but also facilitate a supply of water to the catalytic center (*9*). Due to the proximity of D1-Asp61 with one Mn ion of the Mn-cluster (Mn4 in ref *7*), this residue was proposed to stabilize a water ligand to Mn (*9*). From a series of mutations, Chu et al. (*11*) suggested that D1-Asp61 and D1-Glu65 could influence the properties of the Mn-cluster without significantly affecting its structural features. Clausen et al. (*12*) suggested the importance of D1-Asp61, because the mutation of D1-Asp61 to Asn delayed the half-rise time of O_2 release significantly. These results agree with the position of D1-Asp61 that was found in the neighborhood of the Mn-cluster (*2*, *7*). On the basis of the significant role of CP43-Arg357 in water oxidation (*13*), McEvoy and Brudvig (*14*) further proposed that the proton moving along the exit pathway via D1-Asp61 might be abstracted from a water molecule by CP43-Arg357.

Currently, except for a few of these residues, only limited experimental information on this proton exit pathway is available. To elucidate details of the pathway and its possible role for water oxidation in PSII, we calculated the pK_a for residues along the proposed proton exit pathway by solving the linearized Poisson−Boltzmann (LPB) equation for the whole PSII complex based on the PSII crystal structure at 3.0 Å resolution (*2*), taking into account the atomic coordinates of all amino acid residues and bound cofactors. Here, we focus on the energetics of residues in the proposed proton exit pathway and perform computations under the same conditions and with the same parametrizations as in previous studies (for instance, refs *15*, *16*).

MATERIALS AND METHODS

Atomic Coordinates. In our computations, all atomic coordinates were taken from the crystal structure of PSII from the thermophilic cyanobacterium *Thermosynechococcus elongatus* (*T. elongatus*) at 3.0 Å-resolution (3.0-Å structure, PDB ID 2AXT) (*2*). For comparison, the crystal structure at 3.5-Å resolution (3.5-Å structure, PDB ID 1S5L) (*7*) was also used and, these results are mainly presented in Supporting Information. Hydrogen atom positions were energetically optimized with CHARMM (*17*). During this procedure, positions of all non-hydrogen atoms were fixed and all titratable groups were kept in their standard protonation states, i.e., acidic groups ionized and basic groups (including titratable His) protonated. Simultaneously, Chl*a*, pheophytin *a* (Pheo*a*), and plastoquinone ($Q_{A/B}$) were kept in their neutral charge redox states. His that coordinate Chl*a* were treated as nontitratable with neutral total charge.

Atomic Partial Charges. Atomic partial charges of amino acids were adopted from the all-atom CHARMM22 (*18*) parameter set. To account implicitly for the presence of a proton, the charges of acidic oxygens were both increased symmetrically by +0.5 unit charges. Similarly, instead of removing a proton in the deprotonated state, all hydrogen

charges of the basic groups of Arg and Lys were diminished symmetrically by one unit charge in total. For residues whose protonation states are not available in the CHARMM22 parameter set, appropriate charges were taken from ref *19*.

The exact configuration of the Mn-cluster is still a matter of debate. A Cl^- ion is a potential ligand to the Mn-cluster, although no Cl^- ion was found in the present crystal structures. For the Mn-cluster, we used essentially the same charge model as in previous computations, where we used the former crystal structure at 3.2-Å resolution (PDB ID 1W5C) (*20*) (charges are listed in ref *21*). The latest PSII crystal structure at 3.0-Å resolution (*2*) and the structure at 3.5-Å resolution (*7*) possess an additional Ca^{2+} ion as a part of the Mn-cluster. In our former computations based on the crystal structure at 3.2-Å resolution (but not the crystal structure at 3.5-Å resolution) (*21*), we considered the influence from the Ca^{2+} ion implicitly by increasing the charges of the four Mn ions evenly by 0.5 unit charges. In the present study, we assigned a charge of +2 to the Ca^{2+} ion and lowered the charges of the Mn ions evenly, resulting in the same net charge of the Mn-cluster as in ref *21*. The atomic charges of other redox active cofactors are listed in refs *15*, *16*, and *22*−*24*.

Computation of Protonation Pattern and pK_a. The computation of the energetics of the protonation pattern is based on the electrostatic continuum model by solving the LPB equation with program MEAD from Bashford and Karplus (*25*). To obtain absolute pK_a values of residues in the protein, we calculated the electrostatic energy difference of titratable residues in protein environment and in a suitable reference model system with known experimental pK_a. Cytochrome *b*559 and cytochrome *c*550 were kept in the reduced state. Specifically, unless titrated, Y_Z and Y_D were kept in the neutral charge state.

To sample the ensemble of protonation patterns by a Monte Carlo (MC) method, we used our own program Karlsberg (*26*). For the first 3000 MC scans, random protonation changes were applied for all individual titratable residues. For the remaining 7000 MC scans, titratable residues whose protonation probability deviated by less than 10^{-6} from zero or unity were fixed at the corresponding pure protonation state. The dielectric constant was set to $\epsilon_P = 4$ inside the protein and $\epsilon_W = 80$ for water. All computations were performed at 300 K with pH 7.0 and an ionic strength of 100 mM. The LPB equation was solved using a three-step grid-focusing procedure with a starting, intermediate, and final grid resolution of 2.5, 1.0, and 0.3 Å, respectively. MC sampling yields the probabilities $[A^-]$ and [AH] of the deprotonated and protonated state of the titratable residue A, respectively. With the Henderson−Hasselbalch equation (eq 1),

$$\mathrm{pH} = \mathrm{p}K_a + \log\frac{[A^-]}{[HA]} \qquad (1)$$

the pK_a can be calculated as the pH where the concentration of $[A^-]$ and [AH] are equal. The procedures to obtain the pK_a of titratable residues are equivalent to those of the redox potential for redox-active groups, although in the latter case the Nernst equation is applied instead of eq 1 (*27*). Therefore, the accuracy of the present pK_a computations is directly comparable to that obtained for our recent computations on redox-active cofactors. From the analogy, the numerical error of the pK_a computation can be estimated to be about 0.2 pH units. Systematic errors typically relate to specific conformations that may differ from the given crystal structures and can sometimes be considerably larger. For further information about computational procedure and error estimates, see our previous work for pK_a computation (*15*, *28*, *29*).

Table 1: Calculated pK_a of Residues in the Hydrophilic Channel for Native, PsbO-Deleted (ΔPsbO), PsbU-Deleted (ΔPsbU), and PsbV-Deleted (ΔPsbV) PSII Based on the 3.0-Å structure (*2*)

residues	native S0	native S4	Δ(PsbO)	Δ(PsbU)	Δ(PsbV)
D2 to PsbO					
D2-Lys317[a]	**9.6**[c]	**1.5**	1.4	1.2	1.7
D2-Glu312[a]	4.4	4.2	5.2	4.0	4.3
D1-Glu65[a]	1.8	2.1	3.7	1.8	2.2
PsbO-Arg152	12.6	12.3		12.3	12.3
PsbO-Asp224[a]	9.1	9.0		9.0	9.0
D1 to CP43					
D1-Asp61[a]	**1.1**	**−6.4**	−7.4	−6.7	−6.1
D1-Asp59	**9.3**	**7.1**	**10.2**	6.8	7.3
D1-Arg64	10.9	9.7	**12.4**	9.5	9.8
CP43-Arg343	15.9	15.6	**13.1**	15.6	15.6
CP43					
CP43-Arg357	**15.5**	−1.7	−2.1	−1.9	−1.2
CP43-Asp360	4.6	4.3	3.8	4.3	4.4
D1-His92 (Nδ)[b]	8.4	8.0	8.5	8.1	8.1
CP43-Glu221	5.2	5.1	4.6	5.1	5.1
others					
CP43-Glu348	2.0	1.8	3.6	1.9	1.9
PsbO-Asp158	−1.6	−1.8		−1.9	−1.8

[a] Residues proposed to be involved in the proton exit pathway according to refs *9*, *10*. [b] Due the H-bond between Nϵ(D1-His92) and O_D(CP43-Asp360) (N−O distance 3.1 Å in the 3.0-Å structure (*2*)), Nϵ is permanently protonated. Therefore, we titrated the Nδ site of D1-His92 in the pK_a computation while Nϵ was kept protonated. [c] pK_a values that shifted by more than 2.0 units between the S0 and S4 states are in bold font.

RESULTS AND DISCUSSION

Proton Exit Pathway Overview. Barber, Iwata, and co-workers proposed a cluster of titratable residues in PSII, D1-Asp61, D1-Glu65, D2-Glu312, D2-Lys317 (*7*, *8*) PsbO-Asp158, PsbO-Asp222, PsbO-Asp223, PsbO-Asp224, PsbO-His228, and PsbO-Glu229 (*9*, *10*), to participate in the exit pathway of protons generated during water oxidation. The four residues in D1/D2 are fully conserved. Among the residues in PsbO, Asp158 is fully conserved in all known PsbO sequences. Asp222 and Asp224 are fully conserved, except in PsbO of the ancient cyanobacterium *Gloeobacter violaceus* (*30*). The other PsbO residues, Asp223, His228, and Glu229, are specific for PSII from *T. elongatus*, the cyanobacterium for which the current crystal structures were determined. They are replaced by other polar or titratable residues in PSII from most of the other species (reviewed in ref *10*). In the present study, we focus on residues that are fully or highly conserved from cyanobacteria to higher plants, as summarized in Figure 1.

Our computations indicate a monotonic increase in pK_a of residues along the proton exit pathway from the Mn-cluster in D1/D2 to the lumenal surface in PsbO, except for PsbO-Asp158, which has a very low pK_a value (Table 1). According to these computations we suggest that in addition to the residues proposed by Barber, Iwata, and co-workers

(*7*−*10*) also D1-Asp59, D1-Arg64, and PsbO-Arg152 may participate in the proton exit pathway. These three residues can form the chain of titratable residues with monotonic increase in pK_a, which are located along the proposed proton exit pathway (Table 1, Figure 1). The energetically downhill slope in pK_a along the proton exit pathway is more pronounced in the S4 state than that in the S0 state. In particular, the pK_a of D2-Lys317 at the entrance of the proton exit pathway is downshifted drastically by 8 units (Table 1) upon transition of S0 to S4 state due to the increase of 4 unit charges on the Mn-cluster. For the same reason, the calculated pK_a values for D1-Asp61 and CP43-Arg357 are unusually low in the S4 state, while in the S0 state those pK_a are close to the standard values in aqueous solution. Production of an O_2 molecule from two water molecules at the Mn-cluster in PSII requires 3.2 eV, an enormous amount of energy (reviewed in ref *9*). This energy is provided as oxidation power by the highly accumulated positive charge in the S4 state of the Mn-cluster, which occurs transiently and has not been resolved in spectroscopic studies (reviewed in ref *1*). Therefore, it is not surprising that the residues in the neighborhood of the Mn-cluster possess unusually low pK_a values in the S4 state. Notably, such unusual pK_a shifts were computed only for residues in the immediate vicinity of the Mn-cluster (Table 1, see also Figure 1). On the other hand, the majority of other residues that are likely to participate in the proton exit channel belong to a polar region in PSII such that the influence of the positive charge of the Mn-cluster will be shielded.

The energetics of the titratable residues D1-Asp61, D1-Glu65, D2-Glu312, D2-Lys317, PsbO-Asp158, PsbO-Asp222, and PsbO-Asp224 as well as the three residues D1-Asp59, D1-Arg64, and PsbO-Arg152 suggested in the present study yield a downhill energy proton-transfer pathway starting from D1-Asp61 at the Mn-cluster and terminating at the lumenal surface of PSII independent of the redox state of the Mn-cluster (see Figure 1b). Note that the same proton exit pathway results from the computed pK_a values for the 3.5-Å structure (see supporting Table S1).

There are experimental indications that D1-Asp59, D1-Arg64, and PsbO-Arg152 are associated with water oxidation in PSII. *(i) D1-Asp59:* Mutational studies of PSII from *Synechocystis* sp. PCC 6803 suggested that D1-Asp59 influences the properties of the Mn-cluster as well as D1-Asp61 and D1-Glu65, without significantly affecting the structural stability of the Mn-cluster. In these studies, the D(D1−59)N mutant showed lower light-saturated rates of oxygen evolution, implying that the rate of O_2 release was decreased (*11*). Furthermore, the reduced O_2 release in the D(D1−59)N mutant coincides with a decrease in overall PSII turnover during the S3−[S4]−S0 transitions, suggesting the importance of D1-Asp59 to modulate the redox properties of the higher S-states (*31*). *(ii) D1-Arg64:* The R(D1−64)E mutant of PSII from *Synechocystis* sp. PCC 6803 showed a retarded appearance of O_2 and a pronounced tendency to lose O_2 evolution activity in the dark (*32*). *(iii) PsbO-Arg152:* Mutations of PsbO-Arg152 to Lys in PSII from *T. elongatus* resulted in a significant decrease of the binding affinity of PsbO to the PSII complex and decreased O_2 evolution ability, comparable to mutations of PsbO-Asp158 (*33*). However, mutation of PsbO-Asp158 to Glu, a residue with the same unit charge as Asp, did not affect the PsbO binding affinity to PSII. In contrast, the mutation of PsbO-Arg152 to Lys resulted in a significant decrease in PsbO binding affinity regardless of charge conservation at this residue, indicating the specific requirement of arginine at position PsbO-152 (*33*). The retarded water oxidation and the associated processes for mutations at D1-Asp59, D1-Arg64, and PsbO-Arg152 may be associated with the interruption of the connectivity of the proton exit pathway and indicate the involvement of these three residues in the proton exit pathway.

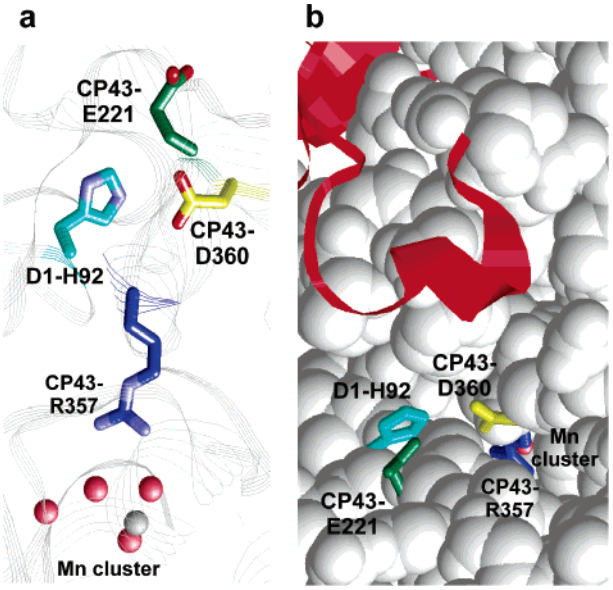

FIGURE 2: Putative water transport channel at the lumenal side, indicated schematically by a small wedge in Figure 1a. Only the side chains of D1-His92 (cyan), CP43-Glu221 (green), CP43-Arg357 (blue), and CP43-Asp360 (yellow) or the component of the Mn-cluster [Mn (pink) and Ca (gray)] are shown with stick or spacefill models. (a) Side view. (b) Top view. Proteins are uniformly depicted with a spacefill model, except for PsbO with a ribbon model.

An Alternative Channel and the Cd^{2+} Binding Site. In the PSII crystal structure (*2*), CP43-Asp360 forms an H bond with D1-His92 (O_D−$N\epsilon_{His}$ distance 3.1 Å) and both of the two residues are exposed to the lumenal bulk surface. D1-His92 is known to influence the catalytic efficiency of the Mn-cluster without significantly affecting the structural stability of the Mn-cluster (*11*), although D1-His92 is 17 Å away from Ca^{2+} in the current crystal structure (*2*). Considering the above-mentioned experimental results and the calculated pK_a values, we propose that another chain of residues CP43-Arg357-CP43-Asp360/D1-His92 may also function as either proton exit pathway for the Mn-cluster or as water intake channel from the bulk. Indeed, there is a relatively large cavity between CP43-Arg357 and CP43-Asp360/D1-His92 at the binding interface between D1 and CP43 (Figure 1). Unlike the interior of the PsbO β-barrel, which is filled by a number of bulky hydrophobic residues (*2*, *7*), this channel is free of bulky hydrophobic residues.

The presence of D1-His92 at the entrance of this channel (Figure 2) is interesting, because His residues are frequently located at the entry point of a proton transport channel (*34*−*36*). A metal ion binding to His of such a channel entry point generally inhibits the physiological function of that channel. These His residues are found at the metal binding sites of

bRC (*34*), cytochrome bc_1 complex (*35*), and cytochrome *c* oxidase (*36*). Thus, in many different enzymes, transport channels employ His residues as entry points due to the proximity of its pK_a with the physiological pH of 7 (reviewed in ref *37*). These structural analogies and similarities let us speculate that the pair of residues CP43-Asp360/D1-His92 form the entry point of the water transport channel at the lumenal side of the PSII complex (Figure 2). The titratable residue closest to CP43-Asp360/D1-His92 is CP43-Glu221, which might be suitable to form the hexagonally coordinated Cd^{2+}-protein complex at the entry point with the other two residues. However, a direct involvement of CP43-Glu221 may be questionable, since CP43-Glu221 is at 8.5 Å from D1-His92 (Figure 2a).

It is known that Cd^{2+} binds to PSII at the electron donor side (O_2 evolving site) (*38*−*40*) and at the electron acceptor side ($Q_{A/B}$ site) (*39*). In connection with the proposed water channel at the donor side, two mechanisms could be considered. One possibility is that metal ions such as Cd^{2+} bind to PSII at the channel entry point, as found in the other photosynthetic proteins. On the basis of Cd^{2+} affinity studies, it was suggested that, among several possible Cd^{2+} binding sites in PSII, a low-affinity site might involve a proton channel or H-bond chain from the catalytic site of water oxidation to the lumenal side of PSII (*39*). Hereby, it is possible that a modified proton release in water oxidation upon Cd^{2+} binding could change the turnover of the redox reactions involving Y_Z and the Mn-cluster (*38*, *39*). If so, then the residues CP43-Asp360/D1-His92 may be the ligands for this Cd^{2+} binding site.

Another possibility is that Cd^{2+} binds competitively to the essential Ca^{2+} site at the Mn-cluster (*38*−*40*). The Mn-cluster is relatively easy to access from the lumenal surface through this alternative channel (Figure 2b). If the pair CP43-Asp360/D1-His92 does not function as Cd^{2+} binding site, the putative water channel may alternatively function as Ca^{2+} intake channel to bind Ca^{2+} at the Mn-cluster. It has been suggested that the lumenal membrane-extrinsic proteins play a role in optimizing the availability of Ca^{2+} and Cl^- for the Mn-cluster (reviewed in ref *41*). Indeed, this channel is located in the vicinity of PsbO (Figure 2). Therefore, it may also be possible that along this channel Ca^{2+} provided by PsbO competes with Cd^{2+} in binding at the Mn-cluster.

Proton Release from Residues during S-State Transitions. The net reaction of water oxidation $2H_2O \rightarrow O_2 + 4H^+ + 4e^-$ indicates that $4H^+$ and O_2 are released from two substrate waters. With higher Mn-cluster oxidation states, the Mn-cluster carries more positive charges. Experimental studies indicate that these positive charges that accumulated at the Mn-cluster during the S-state cycle are partially compensated by proton release (*42*). These protons originate not only from (1) substrate water or its intermediates but also from titratable residues (2) in direct contact (i.e. ligands) with the Mn-cluster or (3) near the Mn-cluster (*43*, *44*) (see discussion in ref *45*). Although a number of reaction schemes and structural models of the Mn-cluster have been proposed, a detailed model based on the crystal structure of the Mn-cluster is yet unavailable. Thus, in the present study, we investigate the protonation pattern of titratable residues in PSII based on each S-state charge model, without evaluating the amount of proton release directly from substrate water in each S state; i.e., we focus on the issue of compensation of the positive charge accumulated at the Mn-cluster (*42*) by the protein environment of PSII. Computation of proton release from PSII would most sensitively depend on subtle details of the S-states charge models. Therefore, it should be noted that the calculated proton release in the present study involves uncertainties that relate to the incomplete atomic coordinates of the Mn-cluster. Because of these uncertainties, we prefer not to provide further details of the pH-dependence of proton release now, although it has been well established that the proton release upon S1 to S2, and S3 to S0 transitions appears to be pH-dependent (*42*, *46*−*48*). This issue can be taken up again once the Mn-cluster and its ligands are known in more detail.

The net-charge compensation in PSII, especially upon the S2 to S3 transition, has been attributed to the expel of a proton from the Mn-cluster (*44*). On the basis of our S-state charge model, we observed for the transition from S2 to S3 a dramatic deprotonation of 0.87 H^+ at CP43-Arg357 (and a small deprotonation of 0.06 H^+ at D2-Glu312 and of 0.09 H^+ at D2-Lys317), resulting in a complete compensation of the unit positive charge appearing at the Mn-cluster by deprotonation of the nearby titratable residues.

On the basis of the PSII crystal structure, CP43-Arg357 has been proposed to be a possible reaction site for the substrate water molecule in the neighborhood of Ca^{2+} (*7*−*9*). Indeed, mutation of CP43-Arg357 to Ser resulted in a PSII with severely inhibited O_2-evolution (*13*). It was further proposed that the proton moving along the exit pathway via D1-Asp61 might be abstracted from the water molecule by CP43-Arg357 (*14*). The change in protonation state for CP43-Arg357 upon S-state transition was proposed to play an important role in water oxidation (*14*). In agreement with a previous proposal of McEvoy and Brudvig (*14*), this residue is fully protonated in the S0 state but fully deprotonated in the higher S states (Table 1).

Upon the S1 to S2 transition we observed deprotonation of 0.81 H^+ at D2-Lys317. The stoichiometry of proton release in this transition (0−0.8 H^+) is known to be smaller than in the S2 to S3 transition (ca. one H^+) (*42*, *46*−*48*). Accordingly, our computation results in pK_a = 6.0 for D2-Lys317, which is lower than 7.8 for CP43-Arg357 in the S2 state. On the other hand, in the higher S-state transition S3 to S4, the largest deprotonation event occurs at D1-Asp59 (by 0.39 H^+) in the present computation. The significant role of D1-Asp59 in O_2 release has been demonstrated in mutational studies (for details, see *Proton Exit Pathway Overview*) (*11*, *31*). This significant deprotonation at D1-Asp59 at higher S states implies its involvement in the proton exit pathway not only geometrically but also electrostatically (for another important aspect of this residue, see the next section). In summary, the present study suggests that deprotonation of CP43-Arg357, D2-Lys317, and D1-Asp59 can play a charge-compensating role in the S-state transitions of PSII.

Two pK_a Values Found with Inhibition of S-State Transitions. It has been well established that the observation of inhibition of S-state transitions goes along with two characteristic pK_a values, the lower one of ∼4−4.5 (for the S2 to S3, S3 to S0, and S0 to S1 transitions) and the higher one of ∼8−10 (for the S2 to S3, and S3 to S0 transitions) (*45*, *46*, *49*). FTIR studies suggested that the lower pK_a value is not attributable to acidic residues that are strongly coupled

to the Mn-cluster (*50*, *51*). In recent FTIR studies it was concluded that this lower pK_a value for the inhibition of the S-state transitions can primarily be related to inhibition of proton release from substrate water and only secondarily be connected to residues participating in the proton exit pathway (*45*). In the present study, D2-Glu312 is the only residue that possesses the pK_a value of 4.2−4.4 throughout the S-state cycle (Table 1) and is not a direct component of the Mn-cluster (Figure 1). Since we did not observe deprotonation of this residue upon S-state transitions, a possible inhibition mechanism of the S-state transitions involving D2-Glu312 would be that its protonation at lower pH energetically blocks the exit pathway for released proton from substrate water.

The observation of the higher pK_a value of ∼8−10 connected with inhibition of the S-state transitions seems to be slightly dependent also on species or preparation conditions (discussed in ref *45*). In PSII-enriched membranes from spinach, inhibition of the S2 to S3 and the S3 to S0 transitions has been suggested to be connected with a pK_a of ∼8−9.4 and was previously assumed to relate to inhibition in electron transfer (ET) from the Mn-cluster to Y_Z due to a decrease of ET-driving energy by downshift of the Y_Z redox potential (E_m) (*49*). On the other hand, in PSII from *T. elongatus*, only the S2 to S3 transition was slightly inhibited, which is connected with a pK_a value of 10.2 ± 1.0 (*45*). From these results, it was proposed that the E_m of the Mn-cluster in PSII from *T. elongatus* was sufficiently lower than $E_m(Y_Z)$ such that the downshift of the $E_m(Y_Z)$ was less crucial to the net driving energy of the ET from the Mn-cluster to Y_Z (*45*). In the present study, two neighboring residues D1-Asp59 and D1-Arg64 share similar pK_a values of ∼8−10.9, which is quite close to the experimentally observed higher pK_a value of ∼8−10 connected with inhibition of the S-state transitions (Table 1; note, the calculated pK_a for D1-Asp59 remains ∼8 except for the S4 state).

In PSII from *Synechocystis* sp. PCC6803, the reduced O_2 release in the D(D1−59)N mutant suggests the importance of D1-Asp59 to modulate the redox properties of the higher S states (*31*). A similar tendency was also observed upon mutation of the neighbor residue D1-Asp61 to Glu (*31*) or to Asn (*52*) (see also Figure 1). Hereby, it is quite notable that mutation of D1-Asp61 to Asn slowed the S1 to S2 and S2 to S3 transitions without affecting the ET from Y_Z to $P680^+$ (*52*). Thus, it is not a change in the $E_m(Y_Z)$ value that is responsible for the observed retardation of S-state transitions. Instead, blocking the proton exit pathway with a mutation of D1-Asp61 can be the origin of the S-state cycle slow-down. Due to the proximity of D1-Asp59 and D1-Asp61 (see Figure 1), it is highly possible that mutation of D1-Asp61 shifts the pK_a of D1-Asp59. Considering these experimental results, we propose that the higher pK_a value of ∼8−10 connected with inhibition of the higher S states is likely to involve deprotonation of a cluster of titratable residues consisting of D1-Asp59 and D1-Arg64, thus rendering the proton exit pathway inefficient.

On the other hand, in the present study D1-Asp61 is always deprotonated, regardless of the S state. Its very low computed pK_a (less than ∼1, Table 1) suggests that this residue can be excluded to directly participate with the higher pK_a value of ∼8−10 connected with inhibition of the higher S states. Nevertheless, due to the proximity of D1-Asp61 with D1-Asp59 (see Figure 1), the protonation states of D1-Asp61 and D1-Asp59 are strongly coupled, probably forming a cluster of interacting residues together with D1-Arg64. Hence, such a cluster of strongly interacting titratable residues hinders a clear assignment of apparent pK_a values to a specific residue, as demonstrated for Glu-L212 and Asp-L213 in bacterial photosynthetic reaction centers from *Rhodobacter sphaeroides* (*28*, *53*−*57*). Thus, we attribute the origin of the higher pK_a value of ∼8−10 connected with inhibition of the higher S states mainly to D1-Asp59 and D1-Arg64, without excluding a secondary contribution from D1-Asp61.

Influence of the Membrane-Extrinsic Proteins on the Energetics of the Proton Exit Pathway. At the lumenal side, at least three proteins are attached to the D1/D2 complex of PSII. One of them, PsbO (33 kDa protein), is conserved in all PSII, showing a moderate primary sequence similarity of 40−50% between cyanobacteria and higher plants. The other two proteins are PsbU/PsbV in cyanobacteria and PsbQ/PsbP in green algae and plants. Regardless of the similarity in association and function, these pairs of proteins differ considerably in their amino acid sequences and structures (see the structures of PsbU in refs *2*, *7*; PsbV in refs *58*, *59*; PsbP in ref *60*; and PsbQ in ref *61*). The membrane-extrinsic proteins PsbO, PsbU, and PsbV have been suggested to optimize the availability of Ca^{2+} and Cl^- for the Mn-cluster. PsbO is also thought to contribute to the structural stability of the Mn-cluster (reviewed in refs *41*, *62*). Thus, these membrane-extrinsic proteins at the lumenal side are closely related to the water oxidation reaction at the Mn-cluster. To investigate the influence of these membrane-extrinsic proteins on the energetics of the proton exit pathway, we calculated the pK_a shifts for these residues after deletion of PsbO, PsbU, or PsbV from the set of atomic coordinates of the PSII crystal structure (*2*, *7*).

The deletion of PsbO dramatically affected the pK_a of these residues, some of which are considered to participate in the proton exit pathway. D2-Glu312 and D1-Glu65 shifted their pK_a by ∼1 unit, and D1-Asp59, D1-Arg64, CP43-Arg343, and CP43-Glu348 by more than ∼2 units (see column ΔPsbO in Table 1). The same level of pK_a shifts is calculated also in the 3.5-Å structure (Table S1 of the Supporting Information). The significant decrease in pK_a of residues in CP43 upon deletion of PsbO may be related to the importance of CP43 in the assembly of the PSII complex, which was suggested to be a prerequisite for PsbO binding to PSII (*63*).

Upon deletion of PsbO, most of these residues, except for D1-Asp59, have more standard pK_a values in contrast to the unusual pK_a values in the presence of PsbO. Indeed, all these residues that change their pK_a upon deletion of PsbO are located at the binding interface of the PSII complex with PsbO, suggesting a strong interference of PsbO binding with the pK_a of those residues involved in the proton exit pathway. Regardless of the significant pK_a shift of the residues, the monotonic increase of pK_a along the proton exit pathway from the Mn-cluster to the lumenal surface is essentially maintained (Table 1). This may suggest that PsbO is not an absolute prerequisite for the energetics of the proton exit pathway, but its presence is necessary to guarantee normal proton exit events. In contrast to PsbO, deletions of PsbU or PsbV do not affect the pK_a of these residues (see column ΔPsbU or ΔPsbV in Table 1). The weak electrostatic influences of PsbU/PsbV on these residues are mainly due

to the large distances of more than 15/18 Å from the nearest residues of the proton exit channel, D1-Glu65/D1-Asp61, respectively.

The significant impact of PsbO binding on the proton exit pathway relative to the small influence of PsbU and PsbV is consistent with the conservation of PsbO in all PSII species. Indeed, among the lumenal membrane-extrinsic proteins of PSII, PsbO seems to be the most crucial to PSII. Enami et al. (*64*) revealed that PsbO isolated from cyanobacteria, red algae, and higher plants is functionally interchangeable, indicating its universal role that is necessary for PSII function. In addition, PSII of the green oxyphotobacterium *Prochlorococcus marinus* possesses the *psbO* gene but lacks genes encoding PsbU and PsbV. On the basis of this finding, De Las Rivas et al. (*62*) suggested that PsbO might be the minimal equipment of membrane-extrinsic proteins required for adequate functioning of water oxidation in PSII. The present study sheds light on the significance of PsbO in its functional role for the energetics of water oxidation in PSII, i.e., tuning the pK_a of residues in the proton exit pathway along D1/D2/CP43/PsbO to foster the reaction efficiently.

SUMMARY

(i) The pK_a computations in the present study suggest that the proton exit pathway for water oxidation in PSII involves a channel formed by D1-Asp61, D1-Glu65, D2-Glu312, D2-Lys317, and PsbO-Asp224.

(ii) In addition, D1-Asp59, D1-Arg64, and PsbO-Arg152 may also participate in the proton-transfer pathway.

(iii) A second channel originates at CP43-Arg357 and terminates at a pair of residues CP43-Asp360/D1-His92 on the lumenal surface. This channel, which putatively functions as either proton exit or water intake channel, may be associated with the Cd^{2+} binding site of PSII.

(iv) Upon transition from S2 to S3, CP43-Arg357 showed a dramatic deprotonation of approximately one H^+.

(v) The calculated pK_a values of 4.2−4.4 for D2-Glu312 and those of ∼8−10.9 for D1-Asp59 and D1-Arg64 may refer to the experimentally determined pK_a values for inhibition of the S-state transitions.

(vi) Among the lumenal extrinsic proteins, PsbO has a significant impact on the pK_a of residues in the proton exit pathway. Hence, a new role of PsbO is suggested: PsbO may also tune the pK_a of the residues in the proton exit pathway, thereby contributing to the efficiency of water oxidation in PSII.

ACKNOWLEDGMENT

We are grateful for valuable discussions with Dr. Michael Haumann. We thank Drs. Donald Bashford and Martin Karplus for providing programs MEAD and CHARMM22, respectively.

SUPPORTING INFORMATION AVAILABLE

This material is available free of charge via the Internet at http://pubs.acs.org.

REFERENCES

1. Goussias, C., Boussac, A., and Rutherford, A. W. (2002) Photosystem II and photosynthetic oxidation of water: An overview, *Philos. Trans. R. Soc. London B 357*, 1369−1381.
2. Loll, B., Kern, J., Saenger, W., Zouni, A., and Biesiadka, J. (2005) Towards complete cofactor arrangement in the 3.0 Å resolution structure of photosystem II, *Nature 438*, 1040−1044.
3. Hoganson, C. W., and Babcock, G. T. (1997) A metalloradical mechanism for the generation of oxygen from water in photosynthesis, *Science 277*, 1953−1956.
4. Vrettos, J. S., and Brudvig, G. W. (2002) Water oxidation chemistry of photosystem II, *Philos. Trans. R. Soc. London B 357*, 1395−1405.
5. Ahlbrink, R., Haumann, M., Cherepanov, D., Bogershausen, O., Mulkidjanian, A., and Junge, W. (1998) Function of tyrosine Z in water oxidation by photosystem II: Electrostatical promotor instead of hydrogen abstractor, *Biochemistry 37*, 1131−1142.
6. Haumann, M., and Junge, W. (1999) Photosynthetic water oxidation: A simplex-scheme of its partial reactions, *Biochim. Biophys. Acta 1411*, 86−91.
7. Ferreira, K. N., Iverson, T. M., Maghlaoui, K., Barber, J., and Iwata, S. (2004) Architecture of the photosynthetic oxygen-evolving center, *Science 303*, 1831−1838.
8. Iwata, S., and Barber, J. (2004) Structure of photosystem II and molecular architecture of the oxygen-evolving centre, *Curr. Opin. Struct. Biol. 14*, 447−453.
9. Barber, J., Ferreira, K., Maghlaoui, K., and Iwata, S. (2004) Structural model of the oxygen-evolving centre of photosystem II with mechanistic implications, *Phys. Chem. Chem. Phys. 6*, 4737−4742.
10. De Las Rivas, J., and Barber, J. (2004) Analysis of the structure of the PsbO protein and its implications, *Photosynth. Res. 81*, 329−343.
11. Chu, H., Nguyen, A. P., and Debus, R. J. (1995) Amino acid residues that influence the binding of manganese or calcium to photosystem II. 1. the lumenal interhelical domains of the D1 polypeptide, *Biochemistry 34*, 5839−5858.
12. Clausen, J., Debus, R. J., and Junge, W. (2004) Time-resolved oxygen production by PSII: Chasing chemical intermediates, *Biochim. Biophys. Acta 1655*, 184−194.
13. Knoepfle, N., Bricker, T. M., and Putnam-Evans, C. (1999) Site-directed mutagenesis of basic arginine residues 305 and 342 in the CP43 protein of photosystem II affects oxygen-evolving activity in *Synechocystis* 6803, *Biochemistry 38*, 1582−1588.
14. McEvoy, J. P., and Brudvig, G. W. (2004) Structure-based mechanism of photosynthetic water oxidation, *Phys. Chem. Chem. Phys. 6*, 4754−4763.
15. Ishikita, H., and Knapp, E.-W. (2005) Oxidation of the non-heme iron complex in photosystem II, *Biochemistry 44*, 14772−14783.
16. Ishikita, H., and Knapp, E.-W. (2005) Control of quinone redox potentials in photosystem II: Electron transfer and photoprotection, *J. Am. Chem. Soc. 127*, 14714−14720.
17. Brooks, B. R., Bruccoleri, R. E., Olafson, B. D., States, D. J., Swaminathan, S., and Karplus, M. (1983) CHARMM: A program for macromolecular energy minimization and dynamics calculations, *J. Comput. Chem. 4*, 187−217.
18. MacKerell, A. D., Jr., Bashford, D., Bellott, R. L., Dunbrack, R. L., Jr., Evanseck, J. D., Field, M. J., Fischer, S., Gao, J., Guo, H., Ha, S., Joseph-McCarthy, D., Kuchnir, L., Kuczera, K., Lau, F. T. K., Mattos, C., Michnick, S., Ngo, T., Nguyen, D. T., Prodhom, B., Reiher, W. E., III, Roux, B., Schlenkrich, M., Smith, J. C., Stote, R., Straub, J., Watanabe, M., Wiorkiewicz-Kuczera, J., Yin, D., and Karplus, M. (1998) All-atom empirical potential for molecular modeling and dynamics studies of proteins, *J. Phys. Chem. B 102*, 3586−3616.
19. Rabenstein, B., Ullmann, G. M., and Knapp, E.-W. (1998) Calculation of protonation patterns in proteins with structural relaxation and molecular ensembles—application to the photosynthetic reaction center, *Eur. Biophys. J. 27*, 626−637.
20. Biesiadka, J., Loll, B., Kern, J., Irrgang, K.-D., and Zouni, A. (2004) Crystal structure of cyanobacterial photosystem II at 3.2 Å resolution: A closer look at the Mn-cluster, *Phys. Chem. Chem. Phys. 6*, 4733−4736.
21. Ishikita, H., Loll, B., Biesiadka, J., Saenger, W., and Knapp, E.-W. (2005) Redox potentials of chlorophylls in the photosystem II reaction center, *Biochemistry 44*, 4118−4124.
22. Ishikita, H., and Knapp, E.-W. (2003) Redox potential of quinones in both electron-transfer branches of photosystem I, *J. Biol. Chem. 278*, 52002−52011.
23. Ishikita, H., and Knapp, E.-W. (2005) Redox potential of cytochrome *c*550 in the cyanobacterium *Thermosynechococcus elongatus*, *FEBS Lett. 579*, 3190−3194.

24. Ishikita, H., and Knapp, E.-W. (2005) Redox potentials of chlorophylls and β-carotene in the antenna complexes of photosystem II, *J. Am. Chem. Soc. 127*, 1963−1968.
25. Bashford, D., and Karplus, M. (1990) pK_a's of ionizable groups in proteins: Atomic detail from a continuum electrostatic model, *Biochemistry 29*, 10219−10225.
26. Rabenstein, B. (1999) *Karlsberg online manual*, http://agknapp.chemie.fu-berlin.de/karlsberg/.
27. Ullmann, G. M., and Knapp, E.-W. (1999) Electrostatic models for computing protonation and redox equilibria in proteins, *Eur. Biophys. J. 28*, 533−551.
28. Ishikita, H., and Knapp, E.-W. (2005) Induced conformational change upon Cd^{2+} binding at photosynthetic reaction centers, *Proc. Natl. Acad. Sci. U.S.A. 102*, 16215−16220.
29. Ishikita, H., Stehlik, D., Golbeck, J. H., and Knapp, E.-W. (2006) Electrostatic influence of PsaC protein binding to the PsaA/PsaB heterodimer in Photosystem I, *Biophys. J. 90*, 1081−1089.
30. Nakamura, Y., Kaneko, T., Sato, S., Mimuro, M., Miyashita, H., Tsuchiya, T., Sasamoto, S., Watanabe, A., Kawashima, K., Kishida, Y., Kiyokawa, C., Kohara, M., Matsumoto, M., Matsuno, A., Nakazaki, N., Shimpo, S., Takeuchi, C., Yamada, M., and Tabata, S. (2003) Complete genome structure of *Gloeobacter violaceus* PCC 7421, a cyanobacterium that lacks thylakoids, *DNA Res. 10*, 137−145.
31. Qian, M., Dao, L., Debus, R. J., and Burnap, R. L. (1999) Impact of mutations within the putative Ca^{2+}-binding lumenal interhelical a−b loop of the photosystem II D1 protein on the kinetics of photoactivation and H_2O-oxidation in *Synechocystis* sp. PCC6803, *Biochemistry 38*, 6070−6081.
32. Li, Z.-L., and Burnap, R. L. (2001) Mutations of arginine 64 within the putative Ca^{2+}-binding lumenal interhelical a−b loop of the photosystem II D1 protein disrupt binding of the manganese stabilizing protein and cytochrome c_{550} in *Synechocystis* sp. PCC6803, *Biochemistry 40*, 10350−10359.
33. Motoki, A., Usui, M., Shimazu, T., Hirano, M., and Katoh, S. (2002) A domain of the manganese-stabilizing protein from *Synechococcus elongatus* involved in functional binding to photosystem II, *J. Biol. Chem. 277*, 14747−14756.
34. Axelrod, H. L., Abresch, E. C., Paddock, M. L., Okamura, M. Y., and Feher, G. (2000) Determination of the binding sites of the proton-transfer inhibitors Cd^{2+} and Zn^{2+} in bacterial reaction centers, *Proc. Natl. Acad. Sci. U.S.A. 97*, 1542−1547.
35. Berry, E. A., Zhang, Z., Bellamy, H. D., and Huang, L. (2000) Crystallographic location of two Zn^{2+}-binding sites in the avian cytochrome bc_1 complex, *Biochim. Biophys. Acta 1459*, 440−448.
36. Aagaard, A., and Brzezinski, P. (2001) Zinc ions inhibit oxidation of cytochrome *c* oxidase by oxygen, *FEBS Lett. 494*, 157−160.
37. Paddock, M. L., Sagle, L., Tehrani, A., Beatty, J. T., Feher, G., and Okamura, M. Y. (2003) Mechanism of proton-transfer inhibition by Cd^{2+} binding to bacterial reaction centers: Determination of the pK_A of functionally important histidine residues, *Biochemistry 42*, 9626−9632.
38. Vrettos, J. S., Stone, D. A., and Brudvig, G. W. (2001) Quantifying the ion selectivity of the Ca^{2+} site in photosystem II: Evidence for direct involvement of Ca^{2+} in O_2 formation, *Biochemistry 40*, 7937−7945.
39. Sigfridsson, K. G. V., Bernat, B., Mamedov, F., and Styring, S. (2004) Molecular interference of Cd^{2+} with photosystem II, *Biochim. Biophys. Acta 1659*, 19−31.
40. Faller, P., Kienzler, K., and Krieger-Liszkay, A. (2005) Mechanism of Cd^{2+} toxicity: Cd^{2+} inhibits photoactivation of Photosystem II by competitive binding to the essential Ca^{2+} site, *Biochim. Biophys. Acta 1706*, 158−164.
41. Seidler, A. (1996) The extrinsic polypeptides of photosystem II, *Biochim. Biophys. Acta 1277*, 35−60.
42. Rappaport, F., and Lavergne, J. (2001) Coupling of electron and proton transfer in the photosynthetic water oxidase, *Biochim. Biophys. Acta 1503*, 246−259.
43. Kodera, Y., Hara, H., Astashkin, A. V., Kawamori, A., and Ono, T.-A. (1995) EPR study of trapped tyrosine Z^+ in Ca-depleted photosystem II, *Biochim. Biophys. Acta 1232*, 43−51.
44. Hundelt, M., Haumann, M., and Junge, W. (1997) Cofactor X of photosynthetic water oxidation: Electron transfer, proton release, and electrogenic behaviour in chloride-depleted Photosystem II, *Biochim. Biophys. Acta 1321*, 47−60.
45. Suzuki, H., Sugiura, M., and Noguchi, T. (2005) pH dependence of the flash-induced S-state transitions in the oxygen-evolving center of photosystem II from *Thermosynechoccocus elongatus* as revealed by Fourier transform infrared spectroscopy, *Biochemistry 44*, 1708−1718.
46. Rappaport, F., and Lavergne, J. (1991) Proton release during successive oxidation steps of the photosynthetic water oxidation process: Stoichiometries and pH dependence, *Biochemistry 30*, 10004−10012.
47. Haumann, M., and Junge, W. (1994) Extent and rate of proton release by photosynthetic water oxidation in thylakoids: Electrostatic relaxation versus chemical production, *Biochemistry 33*, 864−872.
48. Schlodder, E., and Witt, H. T. (1999) Stoichiometry of proton release from the catalytic center in photosynthetic water oxidation, *J. Biol. Chem. 274*, 30387−30392.
49. Bernat, G., Morvaridi, F., Feyziyev, Y., and Styring, S. (2002) pH dependence of the four individual transitions in the catalytic S-cycle during photosynthetic oxygen evolution, *Biochemistry 41*, 5830−5843.
50. Noguchi, T., and Sugiura, M. (2002) Flash-Induced FTIR difference spectra of the water oxidizing complex in moderately hydrated photosystem II core films: Effect of hydration extent on S-state transitions, *Biochemistry 41*, 2322−2330.
51. Noguchi, T., and Sugiura, M. (2003) Analysis of flash-induced FTIR difference spectra of the S-state cycle in the photosynthetic water-oxidizing complex by uniform ^{15}N and ^{13}C isotope labeling, *Biochemistry 42*, 6035−6042.
52. Hundelt, M., Hays, A.-M. A., Debus, R. J., and Junge, W. (1998) Oxygenic photosystem II: The mutation D1-D61N in *Synechocystis* sp. PCC 6803 retards S-state transitions without affecting electron transfer from Y_Z to P_{680}^+, *Biochemistry 37*, 14450−14456.
53. Sebban, P., Maróti, P., Schiffer, M., and Hanson, D. K. (1995) Electrostatic dominoes: Long distance propagation of mutational effects in photosynthetic reaction centers of *Rhodobacter capsulatus*, *Biochemistry 34*, 8390−8397.
54. Gerencsér, L., and Maróti, P. (2001) Retardation of proton transfer caused by binding of the transition metal ion to the bacterial reaction center is due to pK_a shifts of key protonatable residues, *Biochemistry 40*, 1850−1860.
55. Sebban, P., Maróti, P., and Hanson, D. K. (1995) Electron and proton transfer to the quinones in bacterial photosynthetic reaction centers: Insight from combined approaches of molecular genetics and biophysics, *Biochimie 77*, 677−694.
56. Hinerwadel, R., Grzybek, S., Fogel, C., Kreutz, W., Okamura, M. Y., Paddock, M. L., Breton, J., Nabedryk, E., and Mäntele, W. (1995) Protonation of Glu L212 following Q_B^- formation in the photosynthetic reaction center of *Rhodobacter sphaeroides*: Evidence from time-resolved infrared spectroscopy, *Biochemistry 34*, 2832−2843.
57. Nabedryk, E., Breton, J., Okamura, M. Y., and Paddock, M. L. (2004) Identification of a novel protonation pattern for carboxylic acids upon Q_B photoreduction in *Rhodobacter sphaeroides* reaction center mutants at Asp-L213 and Glu-L212 sites, *Biochemistry 43*, 7236−7243.
58. Frazao, C., Enguita, F. J., Coelho, R., Sheldrick, G. M., Navarro, J. A., Hervas, M., De la Rosa, M. A., and Carrondo, M. A. (2001) Crystal structure of low-potential cytochrome c_{549} from *Synechocystis* sp. PCC 6803 at 1.21 Å resolution, *J. Biol. Inorg. Chem. 6*, 324−332.
59. Kerfeld, C. A., Sawaya, M. R., Bottin, H., Tran, K. T., Sugiura, M., Cascio, D., Desbois, A., Yeates, T. O., Kirilovsky, D., and Boussac, A. (2003) Structural and EPR characterization of the soluble form of cytochrome *c*-550 and of the *psbV2* gene product from cyanobacterium *Thermosynechococcus elongatus*, *Plant Cell Physiol. 44*, 697−706.
60. Ifuku, K., Nakatsu, T., Kato, H., and Sato, F. (2004) Crystal structure of the PsbP protein of photosystem II from *Nicotiana tabacum*, *EMBO Rep. 5*, 362−367.
61. Calderone, V., Trabucco, M., Vujicic, A., Battistutta, R., Giacometti, G. M., Andreucci, F., Barbato, R., and Zanotti, G. (2003) Crystal structure of the PsbQ protein of photosystem II from higher plants, *EMBO Rep. 4*, 900−905.
62. De Las Rivas, J., Balsera, M., and Barber, J. (2004) Evolution of oxygenic photosynthesis: Genome-wide analysis of the OEC extrinsic proteins, *Trends Plant Sci. 9*, 18−25.
63. Suorsa, M., Regel, R. E., Paakkarinen, V., Battchikova, N., Herrmann, R. G., and Aro, E.-M. (2004) Protein assembly of

photosystem II and accumulation of subcomplexes in the absence of low molecular mass subunits PsbL and PsbJ, *Eur. J. Biochem. 271*, 96−107.
64. Enami, I., Yoshihara, S., Tohri, A., Okumura, A., Ohta, H., and Shen, J.-R. (2000) Cross-reconstitution of various extrinsic proteins and photosystem II complexes from cyanobacteria, red algae and higher plants, *Plant Cell Physiol. 41*, 1354−1364.

BI051615H